

Model Development and Model-Based Control Design for Nonlinear Smart Composite Systems

AFOSR FA9550-08-1-0348

Final Report

for the period

May 1, 2008 - August 31, 2011

Program Manager:

Fariba Fahroo

AFOSR/RSL

875 North Randolph Street

Suite 325, Room 3112

Arlington, VA 22203

fariba.fahroo@afosr.af.mil

703-696-8429

Principal Investigator:

Ralph C. Smith

Department of Mathematics

North Carolina State University

Raleigh, NC 27695-8205

rsmith@ncsu.edu

919-515-7552

Report Documentation Page

Form Approved
OMB No. 0704-0188

Public reporting burden for the collection of information is estimated to average 1 hour per response, including the time for reviewing instructions, searching existing data sources, gathering and maintaining the data needed, and completing and reviewing the collection of information. Send comments regarding this burden estimate or any other aspect of this collection of information, including suggestions for reducing this burden, to Washington Headquarters Services, Directorate for Information Operations and Reports, 1215 Jefferson Davis Highway, Suite 1204, Arlington VA 22202-4302. Respondents should be aware that notwithstanding any other provision of law, no person shall be subject to a penalty for failing to comply with a collection of information if it does not display a currently valid OMB control number.

1. REPORT DATE 22 NOV 2011	2. REPORT TYPE	3. DATES COVERED 01-05-2008 to 31-08-2011	
4. TITLE AND SUBTITLE Model Development And Model-Based Control Design For Nonlinear Smart Composite Systems		5a. CONTRACT NUMBER	
		5b. GRANT NUMBER	
		5c. PROGRAM ELEMENT NUMBER	
6. AUTHOR(S)		5d. PROJECT NUMBER	
		5e. TASK NUMBER	
		5f. WORK UNIT NUMBER	
7. PERFORMING ORGANIZATION NAME(S) AND ADDRESS(ES) North Carolina State University, Department of Mathematics, Raleigh, NC, 27695		8. PERFORMING ORGANIZATION REPORT NUMBER	
9. SPONSORING/MONITORING AGENCY NAME(S) AND ADDRESS(ES)		10. SPONSOR/MONITOR'S ACRONYM(S)	
		11. SPONSOR/MONITOR'S REPORT NUMBER(S)	
12. DISTRIBUTION/AVAILABILITY STATEMENT Approved for public release; distribution unlimited			
13. SUPPLEMENTARY NOTES			
14. ABSTRACT This program focused on the development of physics-based models, highly efficient numerical approximation techniques, parameter estimation algorithms, and model-based control techniques for shape memory alloys and polymers, electroactive polymers, magnetic actuators, and PZT-based actuators and sensors that provide unique transducer capabilities for Air Force applications. In the modeling and simulation component, energy and statistic-based techniques were used to characterize hysteresis, constitutive nonlinearities, and complex dynamics in a manner that facilitates device and control design. The emphasis in the control component focused on the development of robust linear and nonlinear algorithms that permit real-time implementation while achieving stringent stabilization and tracking specifications.			
15. SUBJECT TERMS			
16. SECURITY CLASSIFICATION OF:			17. LIMITATION OF ABSTRACT Same as Report (SAR)
a. REPORT unclassified	b. ABSTRACT unclassified	c. THIS PAGE unclassified	
			18. NUMBER OF PAGES 14
			19a. NAME OF RESPONSIBLE PERSON

Objectives

This program focused on the development of physics-based models, highly efficient numerical approximation techniques, parameter estimation algorithms, and model-based control techniques for shape memory alloys and polymers, electroactive polymers, magnetic actuators, and PZT-based actuators and sensors that provide unique transducer capabilities for Air Force applications. In the modeling and simulation component, energy and statistic-based techniques were used to characterize hysteresis, constitutive nonlinearities, and complex dynamics in a manner that facilitates device and control design. The emphasis in the control component focused on the development of robust linear and nonlinear algorithms that permit real-time implementation while achieving stringent stabilization and tracking specifications.

Accomplishments

We focused on shape memory alloys, polymers and composites, electroactive polymers, magnetic devices, and lead zirconate titanate (PZT)-based devices due to the unique actuator, sensor and structural capabilities that they provide for present and future Air Force applications. Shape memory alloys (SMA) are presently being considered for vibration attenuation in membrane mirrors and modular antennas, symmetry breaking and flutter control in jet engines, chevrons for improved mixing and flow in jet engines to decrease noise and drag, and MEMs devices for flow control. Shape memory polymers (SMP) provide unique deployment, positioning and vibration attenuation capabilities for payload booms, large-scale mirrors and antennas. Electroactive polymers (EAP) comprised of carbon nanotube infused polyimides are being considered for thin-film membrane mirrors, gossamer antennas and micro-air vehicle (MAV) skins and frames. Finally, PZT-based devices, such as macro-fiber composites (MFC), are being investigated within the context of deployment, positioning and vibration attenuation of large aerospace structures including thin-film membrane mirrors and gossamer antennas. However, all of these compounds exhibit highly nonlinear and hysteretic dynamics that must be incorporated in models and model-based control designs before their potential can be fully realized in Air Force applications.

Development of the Homogenized Energy Model (HEM) Framework for Ferroic Compounds

Through previous AFOSR support, we developed an initial framework for characterizing hysteresis and constitutive nonlinearities in ferroelectric, ferromagnetic and ferroelastic materials which we collectively term ferroic compounds. Representative transducer materials from these material classes are PZT, Terfenol-D and shape shape memory alloys (SMA) such as Nitinol. During the current program, this framework was significantly expanded to provide a unified framework for characterizing the intrinsic coupling between strains, polarization and magnetization. This provides a natural basis for subsequent construction of constitutive relations for devices such as beams, plates, rods, membranes and shells that incorporate PZT, magnetic or shape memory alloy actuators and/or sensors. We summarize here the development from [9] for piezoelectric material to illustrate the general framework.

At the lattice level, we consider the Helmholtz and Gibbs energy densities

$$\psi_\alpha(P, \varepsilon) = \frac{1}{2}\eta_\alpha^\varepsilon(P - P_R^\alpha)^2 + \frac{1}{2}c_\alpha^P(\varepsilon - \varepsilon_R^\alpha)^2 + h_\alpha(P - P_R^\alpha)(\varepsilon - \varepsilon_R^\alpha) \quad (1)$$

and

$$G_\alpha(E, \sigma; P, \varepsilon) = \psi_\alpha(P, \varepsilon) - EP - \sigma\varepsilon \quad (2)$$

where we indicate $\pm 180^\circ$ and 90° orientations by $\alpha = \pm, 90$. Here P, ε, σ , and E respectively denote the polarization, strain, stress and field whereas $P_R, \varepsilon_R, \eta^\varepsilon, c^P$ and h denote the remanence

polarization, remanence strain, inverse susceptibility at constant strain, elastic stiffness at constant polarization, and piezoelectric constant.

For a fixed applied field E and stress σ , the conditions $\frac{\partial G}{\partial P} = 0$ and $\frac{\partial G}{\partial \varepsilon} = 0$ yield the relations

$$\begin{aligned} P_m^\alpha &= P_R^\alpha + \chi_\alpha^\sigma E + d_\alpha \sigma \\ \varepsilon_m^\alpha &= \varepsilon_R^\alpha + d_\alpha E + s_\alpha^E \sigma \end{aligned} \quad (3)$$

where

$$\chi_\alpha^\sigma = \frac{c_\alpha^P}{c_\alpha^P \eta_\alpha^\varepsilon - h_\alpha^2}, \quad d_\alpha = \frac{h_\alpha}{h_\alpha^2 - c_\alpha^P \eta_\alpha^\varepsilon}, \quad s_\alpha^E = \frac{\eta_\alpha^\varepsilon}{c_\alpha^P \eta_\alpha^\varepsilon - h_\alpha^2} \quad (4)$$

are the ferroelectric susceptibility at constant stress, the piezoelectric constant, and elastic compliance at constant field. The minimum of the Gibbs energy in each α -well can then be expressed as

$$G_{\alpha m}(E, \sigma) = -\frac{1}{2} \chi_\alpha^\sigma E^2 - \frac{1}{2} s_\alpha^E \sigma^2 - d_\alpha E \sigma - E P_R^\alpha - \sigma \varepsilon_R^\alpha. \quad (5)$$

The dipole fractions x_+ , x_- and x_{90} associated with positively, negatively, and 90° degree dipoles evolve according to the differential equations

$$\begin{aligned} \dot{x}_- &= -p_{-90} x_- + p_{90-} x_{90} \\ \dot{x}_{90} &= p_{-90} x_- - (p_{90-} + p_{90+}) x_{90} + p_{+90} x_+ \\ \dot{x}_+ &= p_{90+} x_{90} - p_{+90} x_+ \end{aligned} \quad (6)$$

where

$$p_{\alpha\beta}(E, \sigma) = \frac{1}{\tau_{\alpha\beta}} e^{-\Delta G_{\alpha\beta}^a(E, \sigma) V / kT} \quad (7)$$

quantifies the likelihood of transitioning from an α -well to a β -well. Note that (6) can be simplified using the relation $x_+ + x_- + x_{90} = 1$. The activation energy is specified by the relation

$$\Delta G_{\alpha\beta}^a(E, \sigma; F_c) = \begin{cases} \Delta G_0 (1 - F_{\alpha\beta}(E, \sigma) / F_c)^2 & , \quad -F_c \leq F_{\alpha\beta}(E, \sigma) \leq F_c \\ F_c & , \quad F_{\alpha\beta}(E, \sigma) < -F_c \\ 0 & , \quad F_{\alpha\beta}(E, \sigma) > F_c. \end{cases} \quad (8)$$

Here

$$F_{\alpha\beta}(E, \sigma) = G_{\alpha m}(E, \sigma) - G_{\beta m}(E, \sigma) \quad (9)$$

is the thermodynamic driving force. Note that $\Delta G_0 = \frac{1}{4} F_c$ is the energy barrier at zero driving force.

The polarization and strain kernels are given by

$$\bar{P} = \sum_{\alpha=\pm,90} x_\alpha P_m^\alpha, \quad \bar{\varepsilon} = \sum_{\alpha=\pm,90} x_\alpha \varepsilon_m^\alpha. \quad (10)$$

Based on (3), these relations can be expressed as

$$\begin{aligned} \bar{P}(E, \sigma) &= \bar{d}(E, \sigma) \sigma + \chi^\sigma E + \bar{P}_{irr}(E, \sigma) \\ \bar{\varepsilon}(E, \sigma) &= s^E \sigma + \bar{d}(E, \sigma) E + \bar{\varepsilon}_{irr}(E, \sigma) \end{aligned} \quad (11)$$

where

$$\begin{aligned} \bar{d}(E, \sigma) &= \sum_{\alpha=\pm,90} d_\alpha x_\alpha(E, \sigma) \\ \bar{P}_{irr}(E, \sigma) &= \sum_{\alpha=\pm,90} P_R^\alpha x_\alpha(E, \sigma) \\ \bar{\varepsilon}_{irr}(E, \sigma) &= \sum_{\alpha=\pm,90} \varepsilon_R^\alpha x_\alpha(E, \sigma). \end{aligned} \quad (12)$$

In the final step in the development, macroscopic models

$$\begin{aligned} P(E(t), \sigma(t); x_+^0) &= \int_0^\infty \int_{-\infty}^\infty \bar{P}(E(t) + E_I, \sigma(t); F_c) \nu_I(E_I) \nu_c(F_c) dE_I dF_c \\ \varepsilon(E(t), \sigma(t); x_+^0) &= \int_0^\infty \int_{-\infty}^\infty \bar{\varepsilon}(E(t) + E_I, \sigma(t); F_c) \nu_I(E_I) \nu_c(F_c) dE_I dF_c \end{aligned} \quad (13)$$

are constructed by considering interaction fields E_I and thermodynamic driving forces F_c to be manifestations of underlying densities ν_I and ν_c . The final models can thus be expressed as

$$\begin{aligned} P(E, \sigma) &= d(E, \sigma) \sigma + \chi^\sigma E + P_{irr}(E, \sigma) \\ \varepsilon(E, \sigma) &= s^E \sigma + d(E, \sigma) E + \varepsilon_{irr}(E, \sigma) \end{aligned} \quad (14)$$

where

$$\begin{aligned} d(E, \sigma) &= \int_0^\infty \int_{-\infty}^\infty \bar{d}(E_e; F_c) \nu_I(E_I) \nu_c(F_c) dE_I dF_c \\ P_{irr}(E, \sigma) &= \int_0^\infty \int_{-\infty}^\infty \bar{P}_{irr}(E_e; F_c) \nu_I(E_I) \nu_c(F_c) dE_I dF_c \\ \varepsilon_{irr}(E, \sigma) &= \int_0^\infty \int_{-\infty}^\infty \bar{\varepsilon}_{irr}(E_e; F_c) \nu_I(E_I) \nu_c(F_c) dE_I dF_c. \end{aligned} \quad (15)$$

Details regarding various choices for the densities are provided in [9]. For the implementation and parameter estimation algorithms, we employ the representations

$$\begin{aligned} \nu_c(F_c) &= c_1 \sum_{k=k_\alpha}^{K_\alpha} \alpha_k \phi_k(F_c) \quad , \quad \phi_k(F_c) = \frac{1}{\sigma_c^k F_c \sqrt{2\pi}} e^{-[\ln(F_c) - \mu_c]^2 / 2(\sigma_c^k)^2} \\ \nu_I(E_I) &= c_2 \sum_{k=k_\beta}^{K_\beta} \beta_k \varphi_k(E_I) \quad , \quad \varphi_k(E_I) = \frac{1}{\sigma_I^k \sqrt{2\pi}} e^{-E_I^2 / 2(\sigma_I^k)^2} \end{aligned} \quad (16)$$

where

$$c_1 = \left(\sum_{k=k_\alpha}^{K_\alpha} \alpha_k \right)^{-1} \quad , \quad c_2 = \left(\sum_{k=k_\beta}^{K_\beta} \beta_k \right)^{-1} \quad (17)$$

ensure integration to unity. During model calibration, the parameters $\{\alpha_k, \beta_k\}$ are determined through a least squares fit to the data.

To obtain an explicit constitutive equation, we invert the strain relation (14) to obtain

$$\sigma(E, \varepsilon) = c^E \varepsilon - e(E, \sigma_0) E - c^E \varepsilon_{irr}(E, \sigma_0) \quad (18)$$

where

$$c^E = \frac{1}{s^E} \quad , \quad e(E, \sigma_0) = \frac{1}{s^E} d(E, \sigma_0).$$

The constitutive relation (18) can be used to construct rod, beam and shell models for distributed structures. To illustrate, consider a rod having density ρ and cross-sectional area A . Longitudinal displacements are denoted by $u(t, x)$. Force balancing yields

$$\rho A \frac{\partial^2 u}{\partial t^2} = \frac{\partial N}{\partial x}$$

where the force resultant is $N = \sigma A$. The stress is given by (18).

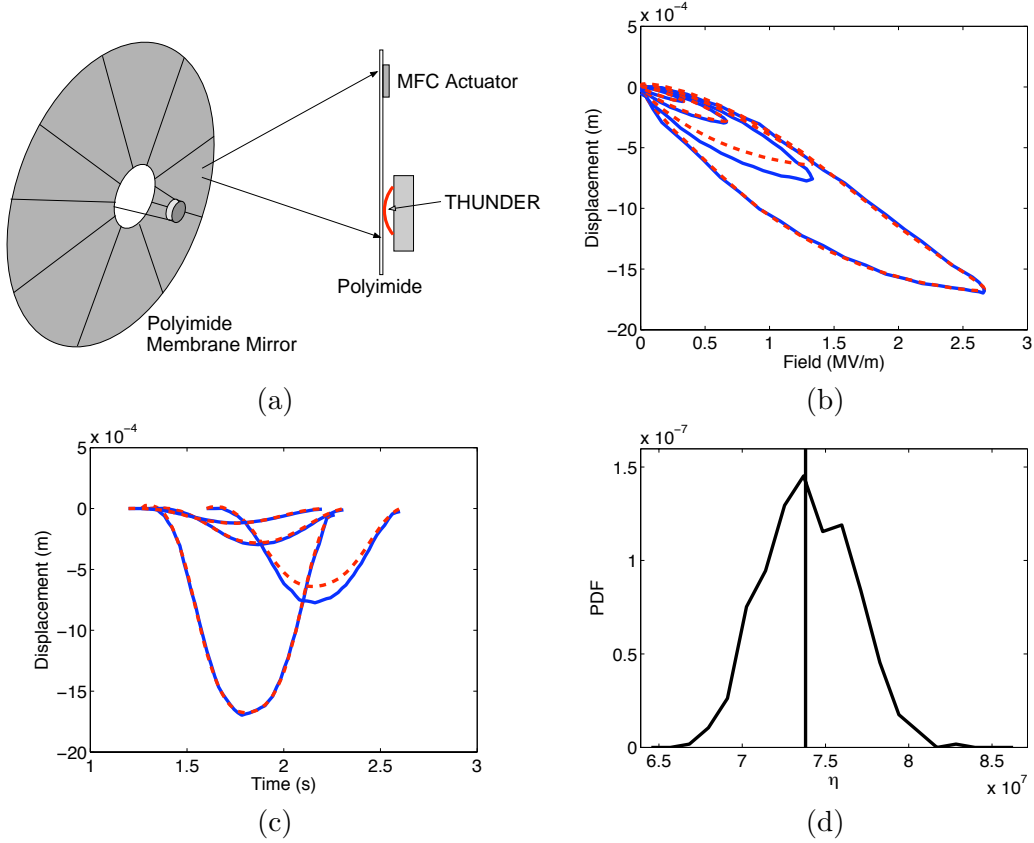


Figure 1: (a) Aerospace application employing macro-fiber composites (MFC). Model fit to 800 VDC experimental data and model predictions for 100, 200 and 400 VDC data in the (b) phase space and (c) time domain. (d) Histogram for the bootstrapped estimate for χ^σ .

For general elastic structures with coupling between the electric and structural components, one would employ the relations

$$\begin{aligned}
 \nabla \cdot D &= 0 \quad , \quad D = \epsilon_0 E + P \\
 \rho \ddot{u} &= \nabla \cdot \sigma \\
 \nabla \times E &= 0 \quad , \quad E = -\nabla \varphi
 \end{aligned} \tag{19}$$

with the vector version of (18).

Details regarding the use of (18) to construct models for PZT-based macro-fiber composite (MFC) actuators operating in highly hysteretic and nonlinear regimes can be found in [11]. Representative model fits are illustrated in Figure 1.

Data-Driven Techniques for Parameter Estimation

To construct the density basis functions $\varphi_k(E_I)$ and $\phi_c(F_c)$, it is necessary to determine values for the driving force mean μ_c and variance σ_c^2 as well as the interaction field variance σ_I^2 . We denote this set of parameters by

$$\bar{p} = [\mu_c, \sigma_c^2, \sigma_I^2]. \tag{20}$$

The remaining parameters are denoted by

$$p = [P_R^+, \varepsilon_R^+, E_R^{90}, \chi^\sigma, d_+, s^E, \gamma, \tau_{90}, \alpha_k, \beta_k]. \tag{21}$$

For the polarization-strain model, this comprises the set that is optimized during model calibration. Structural models require additional elastic and damping parameters.

A critical step when calibrating models is the determination of initial parameter values that facilitate the determination of optimized parameter values through least squares fits to data. A significant aspect of the program focused on the development of data-driven techniques to determine initial parameter estimates based on easily-measured properties of polarization, strain, or magnetization data. Initial results are reported in [1, 4, 10] and this comprises an active component of the present program.

Statistical Model Development, Parameter Estimation, and Model Uncertainty Quantification

During the program, we investigated the development of statistical emulator construction for complex smart systems [18, 19] and initiated the investigation of statistical techniques for parameter estimation and model uncertainty quantification. It is shown in [11] that standard use of asymptotic theory to compute a covariance matrix $V = \sigma^2(\chi^T \chi)^{-1}$, where χ is the sensitivity matrix, is not feasible since the Fisher information matrix $\chi^T \chi$ is singular. Instead we apply bootstrapping methods to determine parameter densities and confidence intervals. As illustrated in Figure 1(d), this permits the determination of non-Gaussian densities that can be used for subsequent model uncertainty quantification.

Model-Based Control Design: Nonlinear Inverse Compensators

The goal of the control component of the investigation was to develop theory and algorithms that permit real-time tracking and vibration attenuation using smart material actuators operating in highly nonlinear and hysteretic regimes. For the applications under consideration, this can result in micron-level (or smaller) tolerances and quasistatic up to kilohertz operating frequencies.

As depicted in Figure 2, there are essentially two control strategies for hysteretic systems using nonlinear models. The first is to use the characterization framework to construct an approximate nonlinear inverse that linearizes the actuator response in the manner depicted in Figure 2(a). Linear control algorithms are then used to achieve control objectives. The second strategy is to construct nonlinear control designs which yield input signals that directly incorporate actuator nonlinearities as depicted in Figure 2(b). The latter strategy is advantageous when tracking trajectories are known *a priori* whereas the inverse compensators will be required when attenuating unmodeled or stochastic uncertainties.

During the grant, we focused significant effort on the development and implementation of \mathcal{L}_1 adaptive control designs for systems employing PZT or magnetic actuators and sensors. As detailed in [5–7], this development employs the following steps. Based on the physical nature of the hysteresis and constitutive nonlinearities, we first assume that inversion errors $\sigma(t)$ are bounded. Projection-based adaptation laws are then constructed using the error $\tilde{x}(t) = \hat{x}(t) - x(t)$ between the states

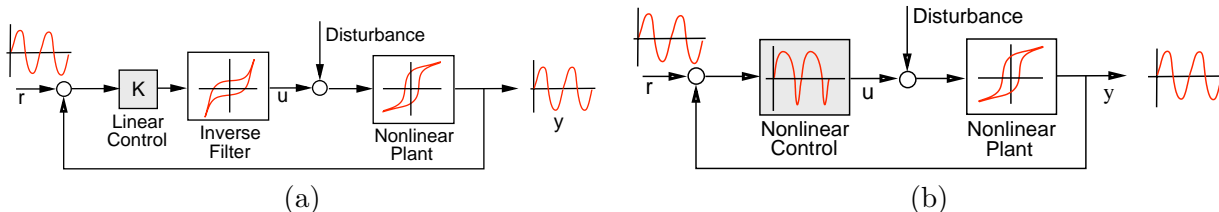


Figure 2: (a) Linear control design employing a nonlinear, model-based inverse compensator and (b) nonlinear model-based control design.

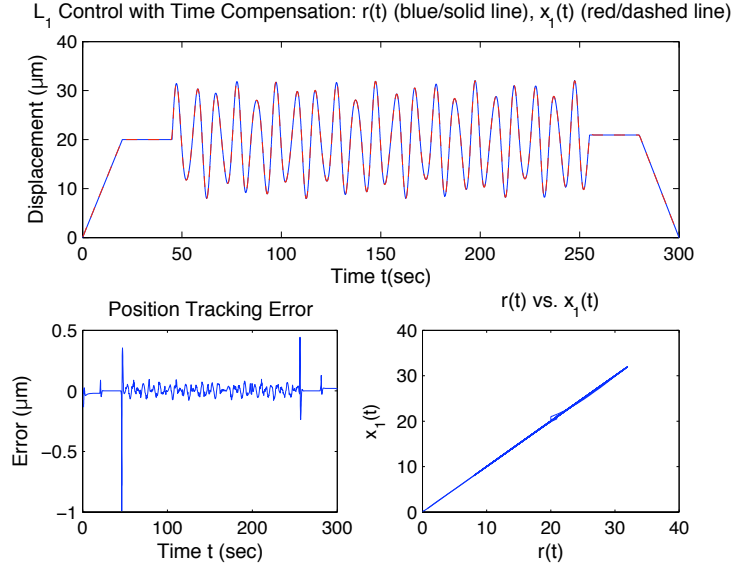


Figure 3: Performance of the \mathcal{L}_1 adaptive control law for tracking a reference signal that includes a ramp, hold, and multiple-frequency component $r(t) = 2 \cos(t) + 10 \cos(\pi t/5)$.

or outputs of the physical and predicted systems. Finally, we incorporate low-pass filters to attenuate high frequency noise. To accommodate constant, filter-induced time delays, we employ time compensation as a final step in the design.

Simulation results illustrating the performance of the method for tracking a reference signal that includes a ramp, hold, and multiple-frequency component $r(t) = 2 \cos(t) + 10 \cos(\pi t/5)$, using a hysteretic PZT-based transducer, are illustrated in Figure 3. It is noted that errors are maintained below a level of $1 \mu\text{m}$ with the maximum errors occurring at points where the derivative in the tracking signal is discontinuous.

Details regarding additional inverse compensator and adaptive control frameworks investigated during this program can be found in [2, 8, 12, 22].

Model-Based Control Design: Nonlinear Perturbation Control

The second main thrust of the control program has focused on the formulation, numerical implementation, and experimental implementation of nonlinear perturbation control designs for systems employing PZT and magnetic actuators operating in hysteretic regimes. As detailed in [15–17], these designs are developed in two steps: (i) construction of an optimal nonlinear open loop control signal, and (ii) construction of a perturbation feedback component.

To illustrate, let r denote a reference signal to be tracked, $y(t) = Cx(t)$ denote observations and let $e(t) = Cx(t) - r(t)$ designate the error. The augmented penalty functional is taken to be

$$\bar{J} = \frac{1}{2} [Cx(t_f) - r(t_f)]^T P [Cx(t_f) - r(t_f)] + \int_{t_0}^{t_f} [\mathcal{H} - \lambda^T(t) \dot{x}(t)] dt \quad (22)$$

where λ denotes the adjoint variable, the Hamiltonian is

$$\mathcal{H} = \frac{1}{2} [e(t)^T Q e(t) + u^T(t) R u(t)] + \lambda^T [Ax(t) + [B(u)](t)], \quad (23)$$

and Q, R respectively penalize large errors and control inputs.

Enforcement of necessary conditions to minimize (22) yields the control input relation

$$u^*(t) = -R^{-1} \left(\frac{\partial B(u)}{\partial u} \right)^T \lambda(t) \quad (24)$$

along with the two-point boundary value problem

$$\dot{z}(t) = F(t, z) \quad (25)$$

where $z = [x, \lambda]^T$ and

$$F(t, z) = \begin{bmatrix} Ax(t) + [B(u)](t) \\ -A^T \lambda(t) - C^T Q C x(t) + C^T Q r(t) \end{bmatrix}. \quad (26)$$

To approximate the solution to (25), we employ a finite difference discretization defined on the grid $t_j = j\Delta t$, where $\Delta t = \frac{t_f}{N}$ and $j = 0, \dots, N$. Letting $z_j \approx z(t_j)$, this yields the discrete system

$$\begin{aligned} \frac{1}{\Delta t} [z_{j+1} - z_j] &= \frac{1}{2} [F(t_j, z_j) + F(t_{j+1}, z_{j+1})] \\ E_0 z_0 &= [x_0, 0]^T \\ E_f z_N &= [0, -C^T P r(t_f)]^T. \end{aligned} \quad (27)$$

The solution of (27) can be expressed as the problem of finding $z_h = [z_0, \dots, z_N]$ which solves

$$\mathcal{F}(z_h) = 0. \quad (28)$$

A quasi-Newton iteration of the form

$$z_h^{k+1} = z_h^k + \xi_h^k, \quad (29)$$

where ξ_h^k solves

$$\mathcal{F}'(z_h^k) \xi_h^k = -\mathcal{F}(z_h^k), \quad (30)$$

is then used to approximate the solution to (28). The Jacobian has the form

$$\mathcal{F}'(z_h) = \begin{bmatrix} S_0 & R_0 & & & & \\ & S_1 & R_1 & & & \\ & & & \ddots & & \\ & & & & S_{N-1} & R_{N-1} \\ E_0 & & & & & E_f \end{bmatrix} \quad (31)$$

where

$$S_i = -\frac{1}{\Delta t} \begin{bmatrix} I & 0 \\ 0 & I \end{bmatrix} - \frac{1}{2} \begin{bmatrix} A & \frac{\partial}{\partial \lambda} B[u_i^*] \\ -C^T Q C & -A^T \end{bmatrix}. \quad (32)$$

The representation for R_i is similar.

It is shown in [15, 16] that an analytic LU decomposition can be determined for $\mathcal{F}(z_h^k)$. This significantly reduces memory requirements and is fundamental for efficient solution.

The open loop control provided by (24) is not robust with regard to model or measurement uncertainties. To provide robustness, we have investigated two perturbation techniques to construct an outer feedback loop: PI and narrowband feedback. The former has the form

$$u_{PI}(t) = -k_p e(t) - k_I \int_0^t e(s) ds,$$

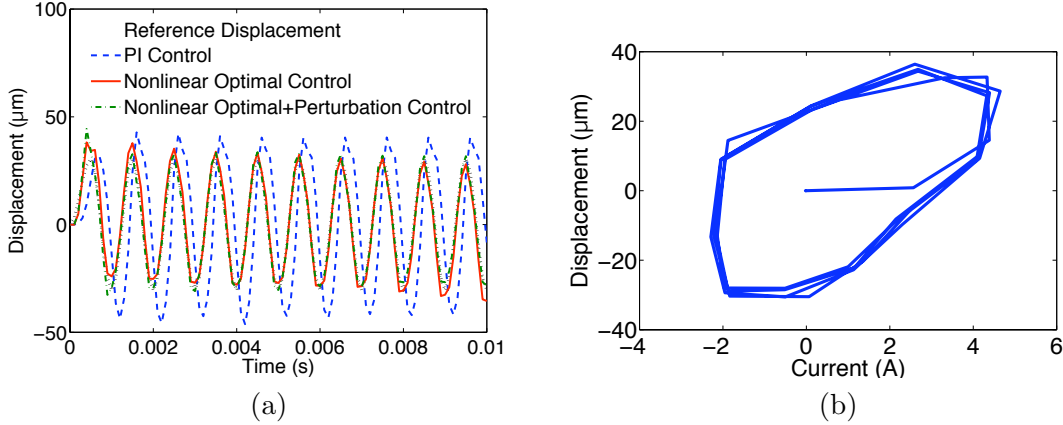


Figure 4: (a) Reference trajectory and experimental tracking performance obtained with PI control, optimal open loop control and perturbation control at 1000 Hz. (b) Hysteretic and nonlinear input-output behavior of the magnetic actuator.

where e denotes measured errors, and provides the advantage that once the open loop control has been computed, it is just as efficient to implement as a straight PI design. We summarize in Figure 4 representative results demonstrating the performance of this perturbation design for a magnetic transducer when experimentally implemented at 1 kHz. It is observed that it provides a significant improvement over PI control at this frequency while operating in a highly hysteretic and nonlinear regime. Further details are provided in [15, 16].

The second perturbation design employs a control law of the form

$$u(t) = u^*(t) + u_{NB}(t) + u_I(t) \quad (33)$$

where $u_I(t)$ provides integral feedback and

$$u_{NB}(t) = -[K_f \ K][x_f; e]$$

is a narrowband feedback term constructed by appending the filter equations

$$\frac{dx_f}{dt} = A_f x_f(t) + BCx(t)$$

to the state. The frequency state matrix has components

$$A_{fi} = \begin{bmatrix} -2\xi_i\omega_i & -\omega_i^2 \\ 1 & 0 \end{bmatrix}$$

where ω_i is a frequency being targeted and ξ_i is the associated damping coefficient; see [20, 21] for details regarding the manner in which hysteretic actuators excite higher harmonic responses.

The performance of this design for a magnetostrictive milling device employed at Etrema Products, Inc., is illustrated in Figure 5. Figure 5(a) demonstrates the model fit for various minor loops with the largest having displacements on the order of 460 μm . The experimental tracking errors achieved when feeding back on various frequency ranges is illustrated in Figure 5(b). Following an initial transient phase, the perturbation feedback design (33) provides tracking errors on the order of 10 μm , thus demonstrating the capability the design for high-accuracy tracking in high-frequency regimes. Further details are provided in [17]. This also represents one aspect of the technology transfer associated with the program.

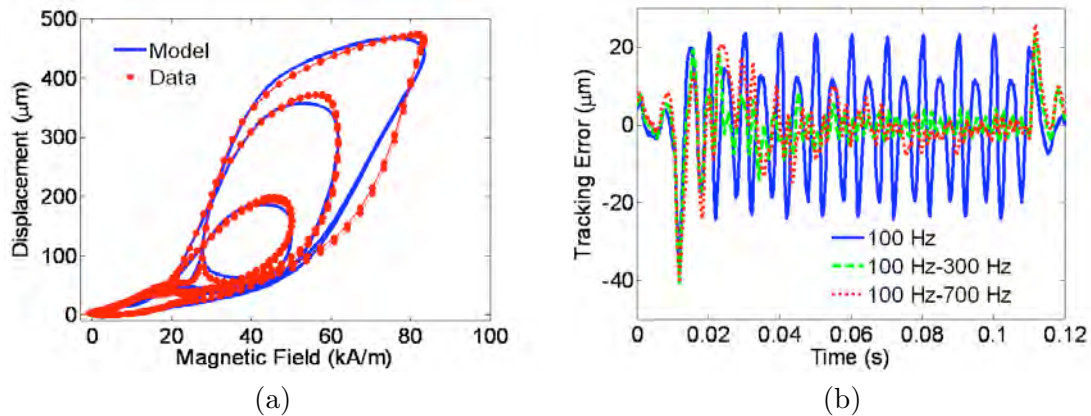


Figure 5: (a) Displacement data and fit of the homogenized energy model. (b) Tracking performance provided by the perturbation design (33) when feeding back on 100 Hz, 100-300 Hz, and 100-700 Hz higher harmonic excitations.

Personnel Supported

Xiang Fan	Graduate Student, NCSU, Raleigh, NC
Emese Lipcsey-Magyar	Graduate Student, NCSU, Raleigh, NC
Stephen May	Graduate Student, NCSU, Raleigh, NC
Jerry McMahon	Graduate Student, NCSU, Raleigh, NC
Jason Scott	Graduate Student, NCSU, Raleigh, NC
Francesca Reale	Graduate Student, NCSU, Raleigh, NC
John Crews	Postdoc, NCSU, Raleigh, NC
Michael Stuebner	Postdoc, NCSU, Raleigh, NC
Ralph Smith	Professor, NCSU, Raleigh, NC

Transitions/Interactions

Transitions

1. *Magnetostrictive Actuators – Etrema*: The nonlinear magnetic constitutive models and perturbation control techniques developed in part through AFOSR support were extended, in collaboration with scientists at Etrema Products, to optimize the performance of Active Machining Systems (AMS) used to mill products such as piston heads [17]. The goal is to significantly increase milling speeds (e.g., up to 20,000 cycles per second) while maintaining micron-level accuracy. The Etrema and AFOSR investigations were mutually complementary and each provides substantial technology transfer to the other. Point of Contact: Rick Zrostlik, Etrema Products Inc., Ames, IA, 515-296-8030.
2. *Shape Memory Polymers – AFRL*: We investigated the development of models, simulation techniques, and control designs for shape memory polymers presently being considered by AFRL researchers for deployment of gossamer structures. The shape memory polymers provide the work density requirements necessary to deploy aerospace structures such as radar antennas and large optical mirrors but exhibit viscoelastic and thermodynamic attributes that are not accommodated by present models or control techniques. Point of contact: Thomas Murphey, Kirtland AFB, Albuquerque, NM, 505-846-9969.

Conference, Colloquia and Workshop Presentations

- Eighteenth International Symposium on Mathematical Theory of Networks and Systems (MTNS 2008), Blacksburg, VA, July 29, 2008.
- Colloquium, Department of Electrical and Computer Engineering, University of Wyoming, Laramie, WY, September 12, 2008.
- Applied Math Seminar, Duke University, Durham, NC, September 22, 2008.
- SPIE's 16th Symposium on Smart Structures and Materials, San Diego, CA, March 9, 2009.
- 2009 U.S. Navy Workshop on Acoustic Transduction Materials and Devices, Penn State University, State College, PA, May 13, 2009.
- SIAM Conference on Control and Its Applications, Denver, CO, July 7, 2010.
- SPIE's 17th Symposium on Smart Structures and Materials, San Diego, CA, March 8, 11 2010 (3 presentations).
- Colloquium, Department of Mathematics, University of Waterloo, Waterloo, Ontario, June 15, 2011.
- Colloquium, Applied Mathematics Department, University of Colorado Boulder, August 27, 2011.
- SPIE's 18th Symposium on Smart Structures and Materials, San Diego, CA, March 7-8k, 2011 (McMahan, Hu).
- Symposium on Hysteresis Modelling and Micromagnetics (HMM 2011), Levico, Italy, May 11, 2011.
- Invited Presentation, 7th Workshop on Control of Distributed Parameter Systems (CDPS 2011), Wuppertal, Germany, July 20, 2011.
- Invited Presentation, SIAM Conference on Control and Its Applications, Baltimore MD, July 25, 2011.

Publicitions Publications resulting from work supported by this grant are listed as references.

References

- [1] J.H. Crews and R.C. Smith, "Density function optimization in the homogenized energy model of shape memory alloys," Proceedings of the ASME 2011 Conference on Smart materials, Adaptive Structures, and Intelligent Systems," to appear.
- [2] M.A. Demetriou, K. Ito and R.C. Smith, "Adaptive techniques for the MRAC, adaptive parameter identification, and on-line fault monitoring and accommodation for a class of positive real infinite dimensional systems," *International Journal of Adaptive Control and Signal Processing*, 23(2), pp. 193-215, 2009.

- [3] L. Downen, T. Glover, L. Hallock, S. King, J. Shor, J. Wallace and R.C. Smith, “Efficient algorithms for implementation of hysteresis models,” Proceedings of the SPIE, Smart Structures and Materials 2009.
- [4] J.M. Ernstberger and R.C. Smith, “Efficient parameter estimation techniques for hysteresis models,” Proceedings of the SPIE, Smart Structures and Materials 2009.
- [5] Xiang Fan, “Model-Based Adaptive Control of Hysteresis in Smart Materials,” PhD Dissertation, North Carolina State University, 2009.
- [6] X. Fan and R.C. Smith, “ \mathcal{L}_1 adaptive control of hysteresis in smart materials,” Proceedings of the SPIE, Smart Structures and Materials 2008.
- [7] X. Fan and R.C. Smith, “Model-based \mathcal{L}_1 adaptive control of hysteresis in smart materials,” Proceedings of the 47th IEEE Conference on Decision and Control, Cancun, Mexico, December 9-11, pp. 3251-3256, 2008.
- [8] X. Fan and R.C. Smith, “Adaptive control design for hysteretic smart systems,” Proceedings of the SPIE, Smart Structures and Materials 2009.
- [9] Z. Hu and R.S. Smith, “A strain model for piezoelectric materials operating in highly hysteretic regimes,” Proceedings of the ASME 2011 Conference on Smart materials, Adaptive Structures, and Intelligent Systems,” to appear.
- [10] Z. Hu, R.C. Smith and J.M. Ernstberger, “Data-driven techniques to estimate parameters in a rate-dependent ferromagnetic hysteresis model,” *Physica B: Physics of Condensed Matter*, to appear; online version: <http://dx.doi.org/10.1016/j.physb.2011.06.084>.
- [11] Z. Hu, R.C. Smith, M. Hays and W.S. Oates, “Statistical parameter estimation and uncertainty quantification for macro fiber composite actuators operating in nonlinear and hysteretic regimes,” 50th IEEE Conference on Decision and Control and European Control Conference, Orlando, FL, December 12-15, 2011, to appear.
- [12] J.A. McMahan and R.C. Smith, “Adaptive control design for hysteretic smart systems,” Proceedings of the SPIE, Smart Structures and Materials 2011.
- [13] S.F. May and R.C. Smith, “Reduced-order model design for nonlinear smart system models,” Proceedings of the SPIE, Smart Structures and Materials 2009.
- [14] S.F. May and R.C. Smith, “Proper orthogonal decomposition with updates for efficient control design in smart material systems,” Proceedings of the SPIE, Smart Structures and Materials 2010.
- [15] W.S. Oates, P.G. Evans, R.C. Smith and M.J. Dapino, “Experimental implementation of a hybrid nonlinear control design for magnetostrictive actuators,” *Journal of Dynamic Systems, Measurement, and Control*, 131, 041004, 2009.
- [16] W.S. Oates and R.C. Smith, “Optimal tracking using magnetostrictive transducers operating in the nonlinear and hysteretic regime,” *Journal of Dynamic Systems, Measurement, and Control*, 131(3), 2009.
- [17] W.S. Oates, R. Zrostlik, S. Eichhorn and R.S. Smith, “A nonlinear optimal control design using narrowband perturbation feedback for magnetostrictive actuators,” *Journal of Intelligent Material Systems and Structures*, 21(16), pp. 1681–1693, 2010.

- [18] F. Reale, “Stastical Emulator Construction for Nonlinear Smart Systems,” Masters Thesis, North Carolina State University, 2009.
- [19] F.D. Reale and R.C. Smith, “Statistical emulator design for nonlinear smart systems,” Proceedings of the SPIE, Smart Structures and Materials 2009.
- [20] M. Stuebner, J. Atulasimha and R.C. Smith, “Frequency response of piezoelectric and magnetostrictive hysteretic nonlinear systems,” Proceedings of SMASIS08, ASME 2008 Conference on Smart Materials, Ellicot City, MD, October 28-30, 2008.
- [21] M. Stuebner, J. Atulasimha and R.C. Smith, “Quantification of hysteresis and nonlinear effects on the frequency response of ferroelectric and ferromagnetic materials,” *Smart Materials and Structures*, 18, 104019, 2009.
- [22] M. Stuebner and R.C. Smith, “Inverse model construction for control implementation of macro fiber composite actuators operating in hysteretic regimes,” Proceedings of the SPIE, Smart Structures and Materials 2010.
- [23] H. Wilson, S. Banda, R.C. Smith and Z. Ounaies, “A continuum model for carbon nanotube-infused polyimides,” Proceedings of the SPIE, Smart Structures and Materials 2009.